pressure [11]. However, some reports have indicated that a change in left ventricular (LV) geometry, especially that resulting from a ventricular septal (VS) shift, leads to decreased RV contractility [11, 12]. A VS shift occurs during treatment with LVADs, especially under full or excess LVAD support [10]. Patients with an LVAD who develop RV failure often have concurrent multiple organ failure [13], for which they require high blood-flow support. Therefore, we often encounter the dilemma that increased RS causes RV dysfunction and consequently decreases systemic blood flow. Ultimately, we implant an RV assist device if a patient does not respond to medical therapy [8]. Ideally, an LVAD should provide not only maximum flow support but also RV functional support.

We consider that a change during the LVAD support phase can control RV function, especially that of the ventricular septum. Hence, we developed a novel heart beat-synchronous drive mode for the EVAHEART centrifugal LVAD (Sun Medical Technology Research Corporation, Nagano, Japan) [14]. To create this drive mode, we defined the duration and rotational speed (RS) of the systolic and diastolic phases to drive the EVAHEART in synchrony with the native cardiac cycle [15–18]. This driving mode, which is synchronous with the heartbeat, significantly changes coronary flow in normal goats [16, 17]. We speculated that a VS shift under continuous-flow LVAD support would occur during the complete cardiac cycle. However, VS function is more essential in the systolic than the diastolic phase and this novel drive mode might confer a benefit on VS and RV function under full bypass conditions by decreasing RS during the systolic phase.

We investigated whether the new drive mode could prevent RV failure in a goat model of bi-ventricular dysfunction and evaluated interaction between the left and right ventricles, including VS movement.

Materials and methods

Animals

Seven adult goats weighing 54.1 ± 2.1 kg were maintained in accordance with the guidelines of the Committee on Animal Studies at the National Cerebral and Cardiovascular Center, and the National Cerebral and Cardiovascular Center Animal Investigation Committee approved the study.

Surgical procedures and implanted devices

All animals were sedated with an intramuscular injection of ketamine hydrochloride (8–10 mg/kg) and anesthetized using isoflurane (1–3 vol %/100 mL in oxygen) inhalation. The animals were placed in the right recumbent position, intubated and mechanically ventilated. We approached the pressure lines for aortic and central venous pressure via a left thoracotomy at the fifth intercostal space from the left intrathoracic artery and vein, respectively. The main pulmonary artery and ascending aorta were dissected and taped, and we attached EMF-1000 electromagnetic flow meters (Nihon Kohden, Tokyo, Japan) with a 12–18-mm diameter to them. After heparinization (300 U/kg), the EVAHEART (Sun Medical Technology Research Corporation, Nagano, Japan) was installed without a cardiopulmonary bypass. First, we sutured the outflow conduit of the device to the descending aorta using a partial clamp. Then we made stitches around the LV apex and punched out the apex with a 16-mm puncher. The inflow cannula was immediately inserted using left hand to control bleeding by squeezing as necessary. We used a 16-mm TS420 ultrasonic flow meter (Transonic Systems, Ithaca, NY, USA) to measure LVAD flow (PF). Total flow (TF) was calculated as the sum of the ascending aortic flow and the PF. The bypass rate was calculated by dividing the PF by the TF.

To obtain pressure–volume loops, we inserted a 6-Fr conductance catheter (2S-RH-6DA-116; Taisho Biomed Instruments Co., Ltd., Osaka, Japan) into the RV from the apex towards the pulmonary valve, and 4-Fr micro-tip catheter pressure transducers (Millar Instruments Inc., Houston, TX, USA) were inserted through the RV and LV walls. In addition, pulmonary artery pressure was monitored via a catheter inserted directly into the artery. Hemodynamic data were recorded using LabChart 7 software (ADInstruments, Castle Hill, New South Wales, Australia). The pressure and volume data of the LV were recorded using a Leycom Sigma 5 system (CardioDynamics, Zoetermeer, The Netherlands). We defined LV and RV systolic duration (%) as the sum of the isovolemic contraction phase and the ejection phase of the respective ventricles divided by the RR interval (Fig. 2). Because blood was ejected during the diastolic phase under LVAD support, we defined the end of ejection phase as the first point when RV volume reached diastolic volume and the first point when the ventricular pressure waveform sharply decreased (Fig. 2). The corresponding systolic duration was measured using LabChart software.

Bi-ventricular dysfunction model

We modeled bi-ventricular dysfunction in this study. We impaired RV and LV function by embolizing the coronary artery through the left anterior descending (LAD) and right coronary (RCA) arteries as described [18]. Briefly, a 4-Fr Amplatz catheter (Create Medic Co., Ltd., Yokohama, Japan) was inserted through a 4-Fr long sheath into the left

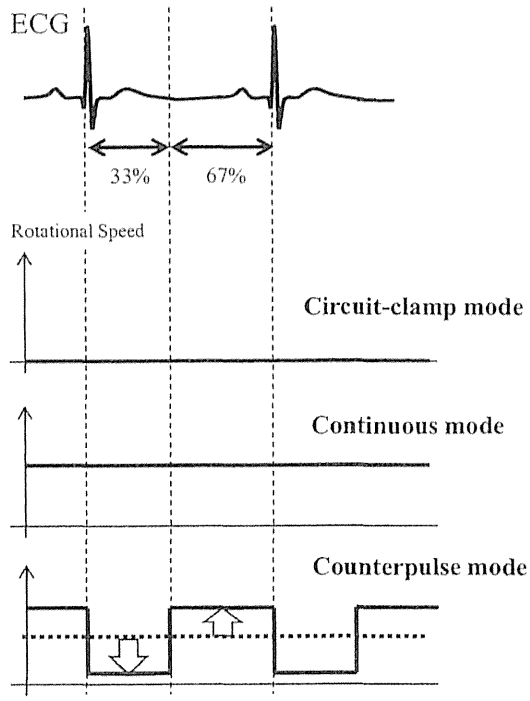

Fig. 1 Rotary blood-pump control modes. Circuit-clamp mode (control) does not include pump support because left ventricular assist device circuit is clamped. Rotational speed in continuous mode remains constant without a controller and that during systolic phase in counter-pulse mode is decreased by a controller. Systolic and diastolic phases in cardiac cycle are defined as 33 and 67 %, respectively, of RR interval

carotid artery toward the LAD and RCA ostia under fluoroscopic guidance. Microspheres (75-μm diameter) were injected into the LAD (60 spheres/kg) and RCA (30 spheres/kg). The general condition of each goat was observed for a further 30 min to stabilize cardiac function before collecting data.

We controlled the infusion volume and depth of anesthesia during the experiment to maintain stable PF and aortic and central venous pressures, thus avoiding suction at the inflow cannula and sustaining an appropriate after load. All animals were administered with lidocaine 2 % (1 mg/kg/h) during the experiment to prevent ventricular arrhythmia. Heart failure was established to reduce and then maintain cardiac output at approximately 60 % of the cardiac output as TF and PAF according to previously described methods [18].

Study protocol and LVAD control

Our new controller allows the RS of the EVAHEART to change for a specific duration after an R wave appears to synchronize it with the cardiac cycle. We defined the systolic and diastolic phases of the cardiac cycle as 33 and 67 % of the RR interval, respectively, (Fig. 1) according to the published protocol [15–18]. The pressure and flow parameters described above were evaluated twice in each goat under the following LVAD controller modes (Fig. 1): circuit-clamp (no pump support due to clamping the LVAD circuit) as the control condition, continuous (constant RS without using the new controller) and counter-pulse (RS decreased during systolic phase using the new controller). We set the RS during the systolic phase to 700–1,000 rpm in the counter-pulse mode and increased the RS in the diastolic phase to achieve an appropriate bypass rate, which was calculated by dividing the PF rate by the sum of the flow rates of the PF and the ascending aorta. We defined full bypass as a rate of about 100 % (range 90–110 %).

Echocardiography

We evaluated RV and LV dimensions by echocardiography using a Vivid E9 system and M5S-D sector transducer (GE Healthcare, Horten, Norway). The end-diastolic and end-systolic RV areas were measured in the direct cardiac long-axis view. The %fractional area change was calculated as:

$$\frac{\text{end} - \text{diastolic RV area} - \text{end} - \text{systolic RV area}}{\text{end - diastolic RV area}} \times 100$$

Statistical analysis

Numerical data are shown as mean ± SE. Differences in values between groups were analyzed by repeated measures analysis of variance followed by Tukey's multiple comparison test. Statistical significance was accepted at a probability value of <0.05. All data were analyzed using SPSS version 19 (SPSS Inc., Chicago, IL, USA).

Results

Bi-ventricular dysfunction models were established by coronary embolism in which TF decreased from 3.3 ± 0.4 to 2.0 ± 0.3 L/min ($p < 0.01$) in the circuit-clamp mode. The dP/dt, particularly in the RV, fell from 436 ± 40 to 341 ± 48 mmHg/s ($p < 0.05$) and E_{max} fell from 1.35 ± 0.16 to 0.87 ± 0.19 ($p < 0.05$) in circuit-clamp mode.

Figure 2 shows sample waveforms of the ECG, R waves, RV pressure, LV pressure, PF, and RS. Actual RS in the counter-pulse mode closely followed the command RS, since average RS in the systolic and the diastolic phase was close. LV pressure waveforms were decreased in the continuous mode. The amplitude of the LV pressure waveforms was similar between counter-pulse and circuit-clamp modes. The duration of the systolic phase differed among the three groups (Fig. 3). The duration of systole

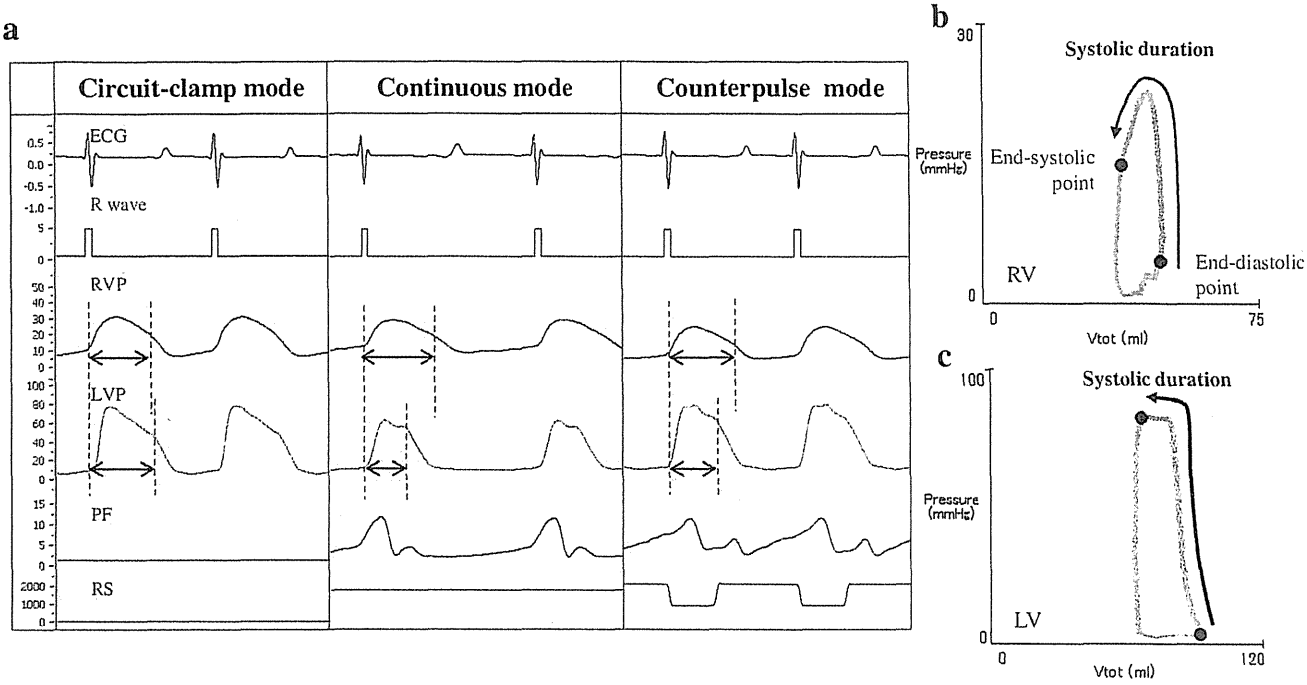

Fig. 2 Sample pressure and flow waveforms and pressure–volume loops for each mode. **a** Left ventricular systolic duration is decreased in continuous mode compared with that in circuit-clamp mode. Duration of LV systolic phase is longer in counter-pulse than in continuous mode. *LV* left ventricular pressure, *PF* pump flow, *RS* rotational speed, *RVP* right ventricular pressure. **b**, **c** Left and right ventricular systolic duration (%) is the sum of isovolumic contraction and ejection phases of respective ventricles divided by cardiac cycle

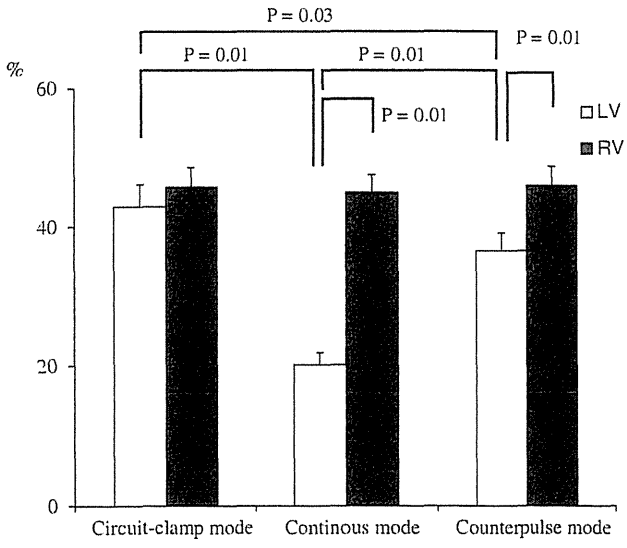

Fig. 3 Systolic duration per mode. Left ventricular systolic phase is significantly shorter than RV systolic phase in continuous mode, and shorter than LV systolic phase in circuit-clamp mode. Left ventricular systolic phase is significantly shorter in counter-pulse than in circuit-clamp mode, and longer than in continuous mode. *LV* left ventricle, *RV* right ventricle

between the right and left ventricles did not significantly differ in circuit-clamp mode (45.8 ± 2.8 vs. 42.9 ± 3.2 %, respectively). The LV systolic phase was significantly shorter than the RV systolic phase in the continuous mode and the LV systolic phase in circuit-clamp mode (LV vs. RV: 20.2 ± 1.8 vs. 45.0 ± 2.5 %, $p = 0.01$). The LV systolic phase was significantly shorter in the counter-pulse, than in the circuit-clamp mode, and significantly longer than in the continuous mode (RV 45.9 ± 2.7 vs. LV 36.5 ± 2.6 %; $p = 0.01$) (Fig. 3).

Table 1 shows the LV and RV data. The LV end-diastolic pressure was significantly decreased in LVAD modes (continuous and counter-pulse modes) compared with circuit-clamp mode. The RV end-diastolic pressure and volume did not significantly differ among the three modes. In addition, pulmonary artery pressure slightly decreased and pulmonary artery flow was slightly higher during the LVAD modes than in circuit-clamp mode, although mean RS in the counter-pulse mode was significantly lower than that of the continuous mode.

RV free wall movement did not significantly change in counter-pulse mode, but VS movement differed among the groups in the direct cardiac short- and long-axis views (Fig. 4). The VS shifted towards the left ventricle in LVAD modes. However, the VS shift was corrected as a result of RS being decreased during the systolic phase in the counter-pulse mode. The end-diastolic RV areas were greater in the LVAD than in circuit-clamp mode. Therefore, the %fractional area change was greater in counter-

Table 1 Hemodynamic data obtained in each drive mode

	Mode		
	Circuit-clamp	Continuous	Counter-pulse
LV			
LVEDP (mmHg)	8.8 ± 1.7	4.7 ± 1.4	4.4 ± 1.2
Mean AoP (mmHg)	59.7 ± 3.0	64.0 ± 3.8	66.0 ± 4.6
Pump flow (L/min)	0.0 ± 0.0	2.4 ± 0.2[a]	2.4 ± 0.2[b]
Total flow (L/min)	2.0 ± 0.3	2.3 ± 0.3	2.3 ± 0.3
Bypass rate (%)	0.0 ± 0.0	107.5 ± 2.4[a]	101.8 ± 3.7[b]
RV			
RVEDP (mmHg)	8.4 ± 1.8	7.9 ± 1.8	8.0 ± 2.0
RVEDV (ml)	75.1 ± 7.8	75.0 ± 8.1	77.8 ± 7.5
d*P*/d*t* max (mmHg/s)	341 ± 48	361 ± 54	381 ± 57
E_{max}	0.87 ± 0.19	0.93 ± 0.22	1.05 ± 0.20
PVA (mmHg/mL)	474 ± 50	522 ± 61	519 ± 50
Mean PAP (mmHg)	27.6 ± 1.9	26.2 ± 0.9	25.4 ± 1.9
PA flow (L/min)	2.1 ± 0.3	2.3 ± 0.3	2.4 ± 0.3
RS			
Actual RS (command RS)			
Systolic RS (rpm)	0 ± 0	1557 ± 53[a] (1588 ± 38[a])	700 ± 23[b,c] (719 ± 12[b,c])
Diastolic RS (rpm)	0 ± 0	1557 ± 53[a] (1588 ± 38[a])	1627 ± 65[b] (1612 ± 46[b,c])
Mean RS (rpm)	0 ± 0	1557 ± 53[a] (1588 ± 38[a])	1290 ± 50[b,c] (1292 ± 36[b,c])

AoP arterial pressure, *LVEDP* left ventricular end-diastolic pressure, *PA* pulmonary artery, *PAP* pulmonary artery pressure, *PVA* pressure volume area, *RS* rotational speed, *RVEDP* right ventricular end-diastolic pressure, *RVEDV* right ventricular end-diastolic volume

[a] $p < 0.01$: circuit-clamp vs. continuous mode

[b] $p < 0.01$: circuit-clamp vs. counter-pulse mode

[c] $p < 0.01$: continuous vs. counter-pulse mode

pulse than in circuit-clamp and continuous modes (59.0 ± 4.6 vs. 56.1 ± 8.8 and 44.7 ± 4.0 %; Fig. 5).

Discussion

To our knowledge, this is the first echocardiographic demonstration of a VS shift being corrected towards the left ventricle in the systolic phase using counter-pulse mode applied to an LVAD. The shift itself might exacerbate RV dysfunction. We consider that LVAD unloading was a major cause of the VS shift, since the duration of the systolic phase was remarkably reduced in continuous mode. The decreased systolic RS provided by the counter-pulse mode significantly corrected LV systolic duration and RV %fractional area change compared with continuous mode. We found that the shortened systolic duration in the continuous mode was corrected in the counter-pulse mode as re-synchronization between the RV and the LV. Thus, we presumed that this favorable effect on RV function was caused by re-synchronizing RV and LV contractions.

Others have discussed the question of whether or not RV function is diminished in patients treated with an LVAD [9–11], especially of the continuous-flow type [7]. We did not find adverse effects on any parameter of RV contractility, such as E_{max}, d*P*/d*t* and pulmonary artery flow. Umeki et al. have demonstrated that the same counter-pulse mode decreases LV end-diastolic volume (LVEDV). They argued the decreased LVEDV and LVEDP directed the unloading effect according to the Staring law. In addition, lower LVEDP decreased RV afterload. However, improvements in RV contractility, such as increased E_{max} or RV diastolic volume, were not evident in counter-pulse compared with continuous mode, although pulmonary flow was slightly increased. In contrast, we confirmed by echocardiography that the novel counter-pulse mode used with the EVAHEART corrected the VS shift during the systolic phase while maintaining a full bypass without a decrease in total systemic flow or adversely affecting the RV. We considered that the counter-pulse mode did not improve RV function because this experiment proceeded under open-chest conditions. That is to say, this mode did not affect the ventricular free wall, which in the right ventricle is important for RV pressure and volume. Taken together, this mode might confer benefits on the right ventricle through the ventricular septum. Park et al. showed that RV performance was impaired by full assist of a left heart bypass with continuous-flow LVAD [10]. Yoshioka et al. [13] discovered that patients with an LVAD who develop RV failure often had concurrent multiple organ failure, for which they required high blood-flow support. We often encounter the dilemma that full LV support causes RV dysfunction and consequently decreases systemic blood flow. Ultimately, some patients required RV assist devices if they did not respond to medical therapy [8]. Our counter-pulse mode can provide not only maximum flow support but also optimized VS movement by only LVADs. We believe that the counter-pulse mode can resolve these issues.

Electrocardiography-synchronized RS control confers several advantages on hemodynamics as well as native heart function compared with continuous RS. Ando et al. [16] created pulsatility using their pulsatile mode with increased RS. Kishimoto et al. [19] reported that speed modulation fully opens the aortic valve and thus prevents aortic insufficiency. Electrocardiography-synchronized RS control of the rotary blood pump confers several beneficial effects compared with the conventional constant RS drive mode. Here, we demonstrated that the system has potential

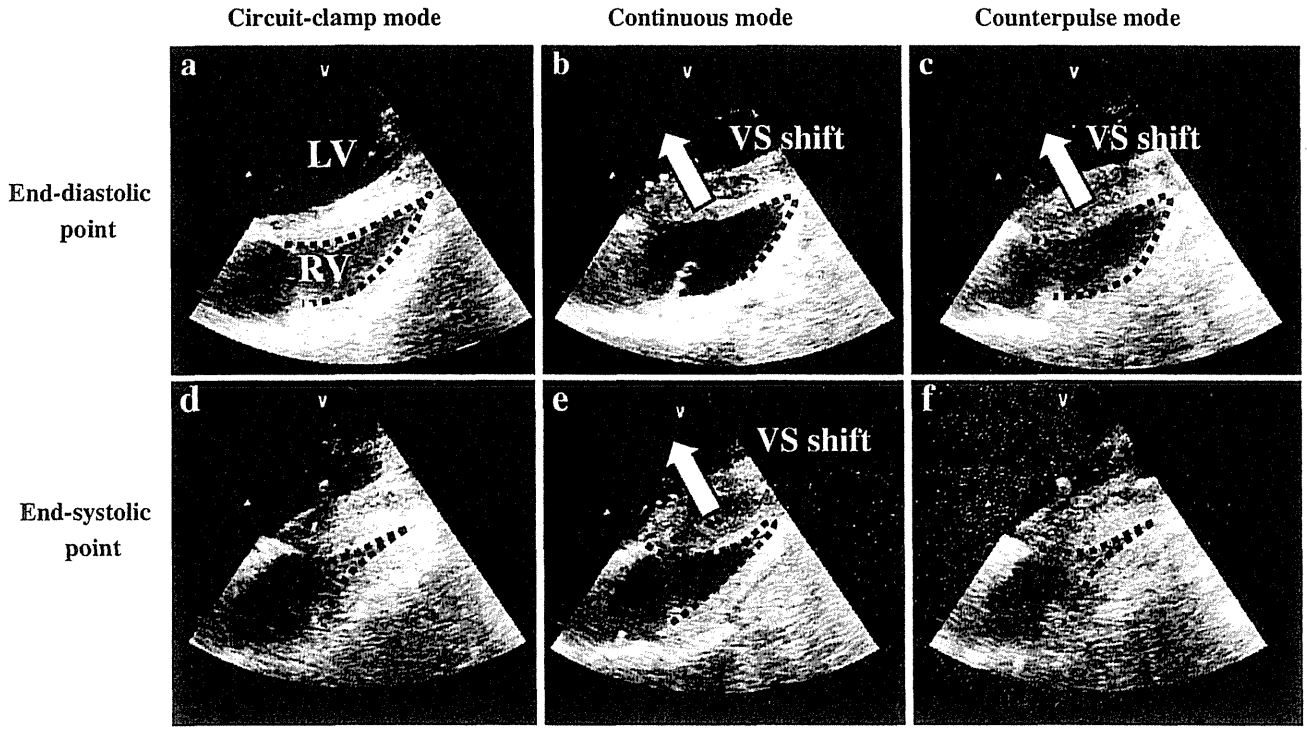

Fig. 4 Sample echocardiograms obtained in each mode. Leftward ventricular septal (VS) shift is evident in continuous and counter-pulse modes (**a**, **b**, **d**, **e**), but corrected by decreased rotational speed during systolic phase in counter-pulse mode (**c**, **f**)

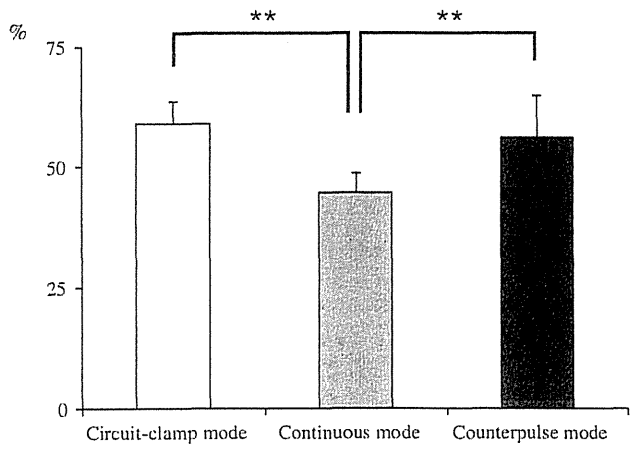

Fig. 5 Bar graph shows right ventricular fractional area change with each mode, $^{**}p < 0.01$

RV support by VS shift correction in addition to the advantages described above. RS control provides further treatment options for circulatory support therapy with rotary blood pumps.

Our study had several limitations. We used an animal model of bi-ventricular dysfunction that developed decreased contractility including that of the ventricular septum. Although VS movement could be evaluated in this model, we could not assess the septal thinning that is a frequent feature of patients with an enlarged LV treated with an LVAD. The next step will be to evaluate VS shift using the new control system in a model with a thin ventricular septum. The experiments proceeded under open-chest condition under which, RV pressure might be difficult to evaluate, since RV pressure remarkably changed according to pressure in the pericardial space. Therefore, the effect of the novel control system should be assessed in a model of chronic heart failure with a thinned ventricular septum under closed-chest conditions.

Conclusion

The novel counter-pulse mode optimized LV unloading and thus corrected VS movement while maintaining sufficient blood flow. This might prevent the RV failure that frequently complicates patients treated with an LVAD, especially during the unstable acute phase after LVAD implantation.

Acknowledgments This study was presented at the annual conference of The American Society for Artificial Internal Organs in 2012, in San Francisco, CA and supported by a JSAO Grant in 2013. The authors are grateful to Dr. Daisuke Ogawa at the Sun Medical Technology Research Corporation for creating the programs.

Conflict of interest The authors have no conflicts of interest to disclose.

References

1. Miller LW, Pagani FD, Russell SD, John R, Boyle AJ, Aaronson KD, Conte JV, Naka Y, Mancini D, Delgado RM, MacGillivray TE, Farrar DJ, Frazier OH, HeartMate II, Clinical investigators. Use of a continuous-flow device in patients awaiting heart transplantation. N Engl J Med. 2007;357:885–96.
2. Lietz K, Long JW, Kfoury AG, Slaughter MS, Silver MA, Milano CA, Rogers JG, Naka Y, Mancini D, Miller LW. Outcomes of left ventricular assist device implantation as destination therapy in the post-REMATCH era: implications for patient selection. Circulation. 2007;116:497–505.
3. Slaughter MS, Rogers JG, Milano CA, Russell SD, Conte JV, Feldman D, Sun B, Tatooles AJ, Delgado RM 3rd, Long JW, Wozniak TC, Ghumman W, Farrar DJ, Frazier OH, HeartMate II Investigators. Advanced heart failure treated with continuous-flow left ventricular assist device. N Engl J Med. 2009;361:2241–51.
4. Garatti A, Bruschi G, Colombo T, Russo C, Lanfranconi M, Milazzo F, Frigerio M, Vitali E. Clinical outcome and bridge to transplant rate of left ventricular assist device recipient patients: comparison between continuous-flow and pulsatile-flow devices. Eur J Cardio Thorac Surg. 2008;34:275–80.
5. Koenig SC, Pantalos GM, Gillars KJ, Ewert DL, Litwak KN, Etoch SW. Hemodynamic and pressure-volume responses to continuous and pulsatile ventricular assist in an adult mock circulation. ASAIO J. 2004;50:15–24.
6. Nishinaka T, Tatsumi E, Nishimura T, Taenaka Y, Masuzawa T, Nakata M, Takano H, Koyanagi H. Cardiac autonomic nervous function during long-term nonpulsatile left heart bypass. Artif Organs. 1999;23:500–3.
7. Patel ND, Weiss ES, Schaffer J, Ullrich SL, Rivard DC, Shah AS, Russell SD, Conte JV. Right heart dysfunction after left ventricular assist device implantation: a comparison of the pulsatile HeartMate I and axial-flow HeartMate II devices. Ann Thorac Surg. 2008;86:832–40.
8. Baumwol J, Macdonald PS, Keogh AM, Kotlyar E, Spratt P, Jansz P, Hayward CS. Right heart failure and "failure to thrive" after left ventricular assist device: clinical predictors and outcomes. J Heart Lung Transplant. 2011;30:888–95.
9. Omoto T, Tanabe H, LaRia PJ, Guererro J, Vlahakes GJ. Right ventricular performance during left ventricular unloading conditions: the contribution of the right ventricular free wall. Thorac Cardiovasc Surg. 2002;50:16–20.
10. Park CH, Nishimura K, Kitano M, Okamoto Y, Ban T. Right ventricular performance is impaired by full assist of left heart bypass. Analysis of right ventricular performance against change in afterload in heart failure models. ASAIO J. 1994;40:M303–8.
11. Kitano M, Nishimura K, Hee PC, Okamoto Y, Ban T. Right ventricular function evaluated by volumetric analysis during left heart bypass in a canine model of postischemic cardiac dysfunction. J Thorac Cardiovasc Surg. 1995;109:796–803.
12. Daly RC, Chandrasekaran K, Cavarocchi NC, Tajik AJ, Schaff HV. Ischemia of the interventricular septum. A mechanism of right ventricular failure during mechanical left ventricular assist. J Thorac Cardiovasc Surg. 1992;103:1186–91.
13. Yoshioka D, Sakaguchi T, Saito S, Miyagawa S, Nishi H, Yoshikawa Y, Fukushima S, Saito T, Daimon T, Ueno T, Kuratani T, Sawa Y. Predictor of early mortality for severe heart failure patients with left ventricular assist device implantation: significance of INTERMACS level and renal function. Circ J. 2012;76:1631–8.
14. Yamazaki K, Kihara S, Akimoto T, Tagusari O, Kawai A, Umezu M, Tomioka J, Kormos RL, Griffith BP, Kurosawa H. EVA-HEART: an implantable centrifugal blood pump for long-term circulatory support. Jpn J Thorac Cardiovasc Surg. 2002;50:461–5.
15. Ando M, Nishimura T, Takewa Y, Ogawa D, Yamazaki K, Kashiwa K, Kyo S, Ono M, Taenaka Y, Tatsumi E. A novel counterpulse drive mode of continuous-flow left ventricular assist devices can minimize intracircuit backward flow during pump weaning. J Artif Organs. 2011;14:74–9.
16. Ando M, Nishimura T, Takewa Y, et al. Electrocardiogram-synchronized rotational speed change mode in rotary pumps could improve pulsatility. Artif Organs. 2011;35:941–7.
17. Ando M, Takewa Y, Nishimura T, Yamazaki K, Kyo S, Ono M, Tsukiya T, Mizuno T, Taenaka Y, Tatsumi E. A novel counterpulsation mode of rotary left ventricular assist devices can enhance myocardial perfusion. J Artif Organs. 2011;14:185–91.
18. Umeki A, Nishimura T, Ando M, Takewa Y, Yamazaki K, Kyo S, Ono M, Tsukiya T, Mizuno T, Taenaka Y, Tatsumi E. Alteration of LV end-diastolic volume by controlling the power of the continuous-flow LVAD, so it is synchronized with cardiac beat: development of a native heart load control system (NHLCS). J Artif Organs. 2012;15:128–33.
19. Kishimoto Y, Takewa Y, Arakawa M, Umeki A, Ando M, Nishimura T, Fujii Y, Mizuno T, Nishimura M, Tatsumi E. Development of a novel drive mode to prevent aortic insufficiency during continuous-flow LVAD support by synchronizing rotational speed with heartbeat. J Artif Organs. 2013;16:129–37.

Alternation of left ventricular load by a continuous-flow left ventricular assist device with a native heart load control system in a chronic heart failure model

Mamoru Arakawa, MD,[a,b] Takashi Nishimura, MD, PhD,[c] Yoshiaki Takewa, MD, PhD,[a] Akihide Umeki, MD, PhD,[d] Masahiko Ando, MD, PhD,[d] Hideo Adachi, MD, PhD,[b] and Eisuke Tatsumi, MD, PhD[a]

Objective: We previously developed a native heart load control system for a continuous-flow left ventricular assist device and demonstrated that the rotational speed synchronized with the cardiac cycle can alter left ventricular preload and myocardial oxygen consumption. In the present study, we assessed this system in a conscious goat model of chronic heart failure.

Methods: Chronic heart failure was induced by coronary microsphere embolization of the left ascending artery and subsequent rapid ventricular pacing in 6 goats. After 4 to 6 weeks of rapid pacing, the goats showed a decreased ejection fraction (from 89.7% ± 3.1% to 53.3% ± 5.4%) measured during sinus rhythm. The assist device was implanted by way of a left thoracotomy, and we examined the effects of the continuous, co-pulse, and counterpulse mode on the end-diastolic volume and stroke work, determined from the left ventricular pressure–volume loops.

Results: Significant decreases were found in the end-diastolic volume and stroke work in the counterpulse mode relative to the values observed with 0% bypass (63.4% ± 15.2% and 39.1% ± 18.2%, respectively; $P < .01$). Furthermore, both increased in the co-pulse mode (82.1% ± 17.6% and 68.3% ± 22.2%; $P < .01$) compared with those in the continuous mode (69.6% ± 15.4% and 54.6% ± 21.6%) with 100% bypass.

Conclusions: The system offers the possibility to control the left ventricular load by changing the rotational speed of a continuous-flow assist device in synchronization with the cardiac cycle. This system should provide the most favorable left ventricular loading conditions for recovery of the native heart. (J Thorac Cardiovasc Surg 2014;148:698-704)

Since continuous-flow left ventricular (LV) assist devices (LVADs) were first approved, the number of patients treated with continuous-flow LVADs has been increasing owing to the improved prognosis and fewer complications.[1,2] Most patients with an implanted LVAD have been on the waiting list for heart transplantation and, thus, have had the LVAD implanted as a bridge to transplantation. However, there is a shortage of donor hearts worldwide, and this shortage has been especially severe in Japan.[3] In some cases, myocardial recovery will allow LVAD explantation, and this has been termed "bridge to recovery" (BTR).[4,5] Because of the extreme shortage of donor hearts, it is important to investigate methods to increase the success rate of BTR. Unloading the left ventricle by an LVAD has been reported to lead to improvement in cardiac function.[4] In contrast, it has also been reported that excess unloading leads to cardiac atrophy.[6] We have presumed that a favorable work load is required for cardiac recovery and that the workload should be adapted to the patient's condition.

We have previously reported the development of novel pump control system for a continuous-flow LVAD (EVAHEART; Sun Medical Technology Research Institute, Nagano, Japan).[7] This system was termed the native heart load control system (NHLCS) and was shown to control the hemodynamic parameters such as pulsatility,[8] myocardial perfusion,[9] and LV end-diastolic volume (LVEDV)[10] by changing the rotational speed (RS) in synchronization with the cardiac cycle.

To evaluate the effects of the NHLCS in detail, it is important to evaluate its long-term performance in a closed-chest animal model with impaired cardiac

From the Department of Artificial Organs,[a] National Cerebral and Cardiovascular Center Research Institute, Osaka, Japan; Department of Cardiovascular Surgery,[b] Jichi Medical University Saitama Medical Center, Saitama, Japan; Department of Cardiac Surgery,[c] Tokyo Metropolitan Geriatric Hospital, Tokyo, Japan; and Department of Cardiothoracic Surgery,[d] University of Tokyo, Tokyo, Japan.

The present study was supported by a grant from Jichi Medical University Graduate School in 2013.

Disclosures: Authors have nothing to disclose with regard to commercial support.

The study was presented at the Annual Conference of the American Society for Artificial Internal Organs, June 15, 2012, San Francisco, Calif.

Received for publication Aug 20, 2013; revisions received Dec 12, 2013; accepted for publication Dec 20, 2013; available ahead of print Feb 9, 2014.

Address for reprints: Mamoru Arakawa, MD, Department of Artificial Organs, National Cardiovascular Center Research Institute, 5-7-1 Fujishiro-dai, Suita, Osaka 565-8565, Japan (E-mail: a_mamoru@mbn.nifty.com).

0022-5223/$36.00

http://dx.doi.org/10.1016/j.jtcvs.2013.12.049

Abbreviations and Acronyms

%LVEDV = LVEDV percentage of the 0% bypass condition
%SW = SW percentage of the 0% bypass condition
BTR = bridge to recovery
EF = ejection fraction
LV = left ventricular
LVAD = LV assist device
LVEDV = LV end-diastolic volume
NHLCS = native heart load control system
PV = pressure–volume
PF = pump flow
RS = rotational speed
SW = stroke work

function.[11] In the present study, we aimed to establish a chronic heart failure model and assess the effect of our EVAHEART on hemodynamics in a conscious animal model of chronic heart failure.

METHODS

Animals

Six adult goats weighing 56.7 ± 5.1 kg were maintained in accordance with the guidelines of the Committee on Animal Studies at the National Cerebral and Cardiovascular Center. The National Cerebral and Cardiovascular Center Animal Investigation Committee approved the present study.

Chronic Heart Failure Model

In the present study, we created chronic heart failure using coronary artery embolization through the left anterior descending coronary artery, as described previously.[10,12] In brief, a 4F Amplatz catheter (Create Medic Co, Ltd, Yokohama, Japan) was inserted through a 4F-long sheath into the left carotid artery toward the left anterior descending coronary artery under fluoroscopic guidance, and 50-μm microspheres were injected (4500/kg). We also placed a permanent pacing lead (Tendril STS, 58 cm, St Jude Medical, Inc, St Paul, Minn) into the right ventricle through the right jugular vein and connected it to a pacemaker (TNT-002N, Taisho Biomed Instruments Co, Ltd, Osaka, Japan) that was implanted subcutaneously in the right shoulder. In addition, we placed an arterial pressure line through the right carotid artery. Four days after embolization, rapid ventricular pacing at 200 beats/min was initiated and continued for 4 to 6 weeks. To control the impairment of cardiac function, we measured the ejection fraction (EF) during sinus rhythm using transthoracic echocardiography (Vivid E9, GE Healthcare, Horten, Norway). The duration of pacing was continued until the EF was reduced to 50% of baseline.

LVAD Implantation

After 48 hours of fasting, all the goats were sedated with an intramuscular injection of ketamine (10 mg/kg). General anesthesia was induced and maintained by inhalation of isoflurane (1%-3% in oxygen). The goats were fixed in the right recumbent position, intubated, and mechanically ventilated. A left thoracotomy along the fifth costal bone was performed, and pressure lines for aortic pressure and central venous pressure measurement were placed into the left intrathoracic artery and vein, respectively. This was followed by attachment of an electromagnetic flow meter (EMF-1000, 17-20 mm in diameter, Nihon Kohden, Tokyo, Japan) around the ascending aorta. After heparinization (200 U/kg), the centrifugal LVAD (EVAHEART; Sun Medical Technology Research Corp, Nagano, Japan) was installed by punching out the LV apex with a 16-mm puncher, inserting the inflow cannula into the left ventricle and suturing the outflow conduit (16-mm J Graft SHIELD NEO, Japan Lifeline, Tokyo, Japan) into the descending aorta. We used an ultrasonic flow meter (16 mm; TS420, Transonic Systems, Ithaca, NY) to measure the LVAD pump flow (PF). After establishing the pump circuit, we attached 2 ultrasonic crystals (Sonometrics, Ontario, Canada) in the anterior and posterior endocardium to measure the LV diameter in the short axis. This diameter was then used to calculate the LV volume using a single-axis sphere. In addition, a LV pressure line was inserted from the anterior wall.

Study Protocol and LVAD Control

Two days after LVAD implantation, when the goats had recovered from the acute effects of the operation, we tested 3 drive modes using our previously described NHLCS.[10,12] With this controller, we were able to change the RS of the EVAHEART for a specific period after the occurrence of an R wave to synchronize it with the cardiac cycles. We defined the systolic phase as 30% of the RR interval, and the diastolic phase as 65% of the RR interval. These parameters were evaluated twice in each goat using the following 3 conditions: (1) the continuous mode (constant RS without the use of the novel controller); (2) the co-pulse mode (increased RS in the systolic phase and decreased RS in the diastolic phase using the novel controller); and (3) the counterpulse mode (decreased RS in the systolic phase and increased RS in the diastolic phase with the novel controller). In these drive modes, we set the RS from 1500 to 3000 rpm to achieve a proper bypass rate. In addition, the difference between the systolic and diastolic phase was set to approximately 500 to 1000 rpm.

Statistical Analysis

The bypass rate was calculated by dividing the pump flow (PF) rate by the sum of the PF and ascending aortic flow rates. We defined full bypass as a bypass rate of 100%. We tested the 3 drive modes at bypass rates of 50%, 75%, and 100% for 10 minutes. Next, we performed the 3 modes at a bypass rate of 100% for 12 hours to evaluate the effects of the system for a prolonged period. To evaluate appropriate support, we checked the actual RS and speed changes. The bypass rate was calculated in real time and displayed on a monitor.

The hemodynamic data were recorded using Labchart, version 7, software (ADInstruments, Castle Hill, Australia). The implanted ultrasonic crystals provided the LV chamber diameter in the short axis, and this was used to estimate the LV volume from a single-axis spherical model. LV pressure–volume (PV) loops were drawn for each mode, and the stroke work (SW) was calculated from the area inside the PV loop using CardioSOFT (Sonometrics). The LV end-diastolic pressure and LVEDV were determined from the PV loops. For the comparison between each control mode, the LVEDV and SW are expressed as percentages of the 0% bypass condition (%LVEDV and %SW, respectively).

All numeric data are shown as the average ± standard deviation. The data between pre-embolization and pre-LVAD implantation were compared using a paired Student's t test. Other comparisons between the groups were performed using repeated measures analysis of variance followed by Tukey's multiple comparison tests. All analyses were performed using the Statistical Package for Social Sciences, version 19 (SPSS Inc, Chicago, Ill).

Effect of LVAD on Hemolysis and Myocardial Histologic Findings

To evaluate hemolysis, we measured free hemoglobin before and after the 3 modes had been applied for 12 hours in 1 of 6 goats. In addition, an

in vitro hemolysis test was performed, with mock circulation, according to a previous report.[13] Fresh bovine blood (600 g) was used, and the blood temperature was maintained at 37° ± 1°C. Blood samples were collected for measurement of plasma free hemoglobin just after the pump's condition had become stable and at 30-minute intervals for 4 hours. We drove the EVAHEART in the co-pulse mode at a pulse rate of 60 beats/min. The RS was set 3000 rpm for high and 1000 rpm for the difference. These settings were representative of the most severe condition of the novel mode. The mean head pressure was set at 100 mm Hg and the PF at 5.0 L/min for the continuous and co-pulse modes both. These settings were the same as those in a previous report.[13] We used the normalized index of hemolysis to evaluate hemolysis: normalized index of hemolysis (g/100 L) = Δ plasma free hemoglobin (g/L) × priming volume (L) × ([(100 − hematocrit)/100] × [100/PF in L/min × time in minutes]). We performed biopsy from the apex during LVAD implantation and necropsy when the goats had been killed 1 month after LVAD implantation to evaluate the pathologic changes due to LVAD implantation. The samples were fixed immediately in 10% neutral-buffered formalin and embedded in paraffin wax. Thin sections were cut and stained with hematoxylin and eosin.

RESULTS

Chronic Heart Failure Model With LVAD Support

We performed rapid pacing for 31.4 ± 5.7 days. The EF, measured by echocardiography, decreased from 89.7% ± 3.1% at the pre-embolization baseline to 53.3% ± 5.4% just before LVAD implantation ($P < .01$).

Hemodynamic and LVAD Data

Figure 1 shows sample waveforms from the electrocardiogram, aortic pressure, detected R waves, LV pressure, PF, native flow, and RS. Important differences were present among the PF waveforms with the 3 different modes. The maximum PF increased after an increase in the RS in the systolic phase in the co-pulse mode compared with that in the continuous mode. In contrast, the PF in the diastolic phase increased in the counterpulse mode compared with that in the continuous mode. The hemodynamic data in each mode are listed in Table 1. The heart rate, central venous pressure, aortic pressure, total flow, and bypass rate were not significantly different among the 3 modes. The average RS in the counterpulse mode decreased significantly compared with those in the continuous and co-pulse modes at each bypass rate.

PV Loops

Figure 2 shows 1 sample set of PV loops for each mode. The horizontal axis shows the LV volume and the vertical axis the LV pressure. The lower right points indicate the end-diastolic points, and the area inside the loop indicates the SW. The LVEDV (preload) increased in the co-pulse mode and decreased in the counterpulse mode compared with that in the continuous mode.

Figure 3 shows the average LVEDVs measured in the 6 goats. The %LVEDV and %SW were decreased according to the decrease in the bypass rate in the continuous mode. The %LVEDV was significantly increased in the co-pulse mode compared with that in the continuous mode at the 75% bypass rate. SW was also increased in the co-pulse mode compared with that in the continuous mode at the 75% and 100% bypass rates. Furthermore, the %LVEDV was significantly increased in the co-pulse mode compared with that in the counterpulse mode at each bypass rate. The %SW was also increased in the co-pulse mode compared with that in the counterpulse mode at each bypass rate. In the counterpulse mode, the %LVEDV and %SW were relatively lower than those in the continuous mode, although the differences were not significant.

Appropriate Support

To check for appropriate support, we evaluated 7688 ± 400 beats/h, on average. Appropriate support was achieved for >90% of cardiac beats in 1 hour. The most frequent cause of inappropriate support was a failure to sense the R wave by the controller (4.4%).

Effect of LVAD on Hemolysis and Myocardial Histologic Findings

The free hemoglobin in vivo showed a slight elevation after each mode of pumping. The hemoglobin values before and after each mode were 2.7 and 5.2 mg/dL in the continuous mode, 5.2 to 5.9 mg/dL in the co-pulse mode, and 4.2 and 6.4 mg/dL in the counterpulse mode, respectively. Regarding the in vitro hemolysis test, plasma free hemoglobin was slightly increased in the samples collected after the pump had run for 4 hours in the continuous and co-pulse modes both. The hemoglobin values just after the pump's condition had become stable and after 4 hours of pumping in each mode were 0.6 and 3.4 mg/dL in the continuous mode, 3.4 to 5.0 mg/dL in the co-pulse mode, and 4.2 mg/dL and 6.4 mg/dL in the counterpulse mode, respectively. However, the normalized index of hemolysis was not different between the continuous and co-pulse modes (0.000944 vs 0.000843, respectively). In addition, we found focal myocardial fibrosis (Figure 4, *A* and *C*), but this was not affected by LVAD implantation. No remarkable change was found in the cardiomyocyte size after support with this system, although the mode was switched in each goat (Figure 4, *B* and *D*).

DISCUSSION

For the first time, we have reported an evaluation of the effects of the NHLCS in a chronic heart failure model. To our knowledge, several reports have evaluated the effects of a control system with electrocardiogram-synchronized RS changes.[8,10,12,14-16] However, our study is the first to evaluate this system in a conscious animal model of chronic heart failure. Our results have indicated the feasibility of the long-term use of this system. Thus, our results provide information regarding what might be expected when this system is used in the clinical setting.

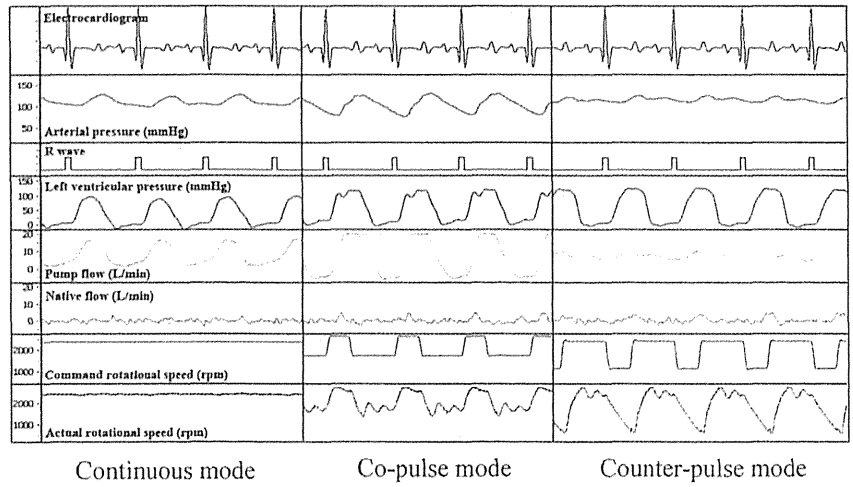

FIGURE 1. Sample pressure and flow waveforms at full bypass in each mode. In the co-pulse mode, the pump flow increased in the systolic phase, which was followed by an increase in the rotational speed (RS). In contrast, in the counterpulse mode, the pump flow had increased in the diastolic phase, followed by an increase in the RS compared with the continuous mode.

Furthermore, the results showed no adverse events such as an increase of hemolysis or myocardial overload, and the system provided reliable support.

According to a previous report, unloading of the left ventricle is a factor that promotes cardiac recovery.[4] However, we have assumed that unloading is not the only factor that promotes cardiac functional recovery. Excessive unloading of the left ventricle by an LVAD could lead to cardiac disuse atrophy.[6] Furthermore, clenbuterol, a β_2-receptor agonist, has been reported to increase the success rate of BTR.[17,18] From these findings, a favorable cardiac workload for the native heart according to the patient's condition should be considered to achieve optimal cardiac recovery. Because the co-pulse mode can provide active LV load management, the native heart can contract by itself in this mode; therefore, it acts as the cardiac training mode. The counterpulse mode can decrease the LV load. In the counterpulse mode, the native heart can rest, but systemic assistance is maintained. Therefore, it can be used as a cardiac resting mode.

Umeki and colleagues[10,12] demonstrated the ability of the newly developed NHLCS to control the LVEDV and myocardial oxygen consumption. These parameters were increased in the co-pulse mode and decreased in the counterpulse mode in those studies. Our results were largely similar to theirs, although several differences were present. First, we required a higher RS speed to achieve the target bypass rate, because the mean blood pressure was greater

TABLE 1. Hemodynamic data

	50% Bypass rate			75% Bypass rate			100% Bypass rate		
Variable	Continuous mode	Co-pulse mode	Counterpulse mode	Continuous mode	Co-pulse mode	Counterpulse mode	Continuous mode	Co-pulse mode	Counterpulse mode
HR (beats/min)	126.0 ± 16.4	128.7 ± 16.5	126.0 ± 15.7	128.5 ± 16.8	128.8 ± 19.7	127.6 ± 18.1	126.0 ± 15.6	128.7 ± 16.5	126.8 ± 16.4
Mean CVP (mm Hg)	−3.2 ± 2.9	−3.0 ± 2.8	−2.1 ± 3.2	−3.4 ± 3.4	−2.8 ± 4.2	−3.8 ± 4.3	−2.5 ± 3.2	−1.6 ± 3.3	−3.3 ± 3.9
Mean AoP (mm Hg)	87.2 ± 21.3	83.7 ± 19.1	87.0 ± 20.6	87.8 ± 18.2	86.4 ± 20.3	92.0 ± 21.0	94.4 ± 20.0	91.2 ± 19.9	95.0 ± 20.2
PF (L/min)	2.0 ± 0.6*,†	2.1 ± 0.6*,†	2.0 ± 0.6*,†	3.3 ± 1.2†,‡	3.2 ± 1.0†,‡	3.2 ± 0.8†,‡	4.3 ± 1.1*,‡	4.3 ± 1.4*,‡	4.2 ± 1.0*,‡
Total flow (L/min)	3.9 ± 1.3	3.9 ± 1.3	3.9 ± 1.3	4.3 ± 1.5	4.3 ± 1.3	4.2 ± 1.2	4.1 ± 1.2	4.0 ± 1.4	4.0 ± 1.3
RS (rpm)	1648 ± 116*,†	1721 ± 295*,†	1563 ± 158*,†	1890 ± 134†,‡,§	1852 ± 177†,‡,§	1637 ± 164†,‡,‖,¶	2046 ± 102*,‡,§	1941 ± 276*,‡	1783 ± 204*,‡,¶
Bypass rate (%)	51.2 ± 4.3*,†	53.3 ± 4.5*,†	52.6 ± 4.0*,†	75.0 ± 3.2†	76.3 ± 2.7†,‡	75.5 ± 5.6†,‡	100.0 ± 4†,‡	101.6 ± 9.3*,‡	96.9 ± 8.7*,‡
LVEDP (mm Hg)	14.7 ± 9.3	15.5 ± 9.9	11.8 ± 9.5	9.3 ± 7.9	15.3 ± 9.1	7.6 ± 8.6	7.7 ± 7.7	10.9 ± 8.5	7.2 ± 7.8

HR, Heart rate; *CVP*, central venous pressure; *AoP*, aortic pressure; *PF*, pump flow; *RS*, rotational speed; *LVEDP*, left ventricular end-diastolic pressure. *Compared with 75% with the same mode. †Compared with 100% with the same mode. ‡Compared with 50% with the same mode. §Compared with counterpulse mode. ||Compared with continuous mode. ¶Compared with co-pulse mode.

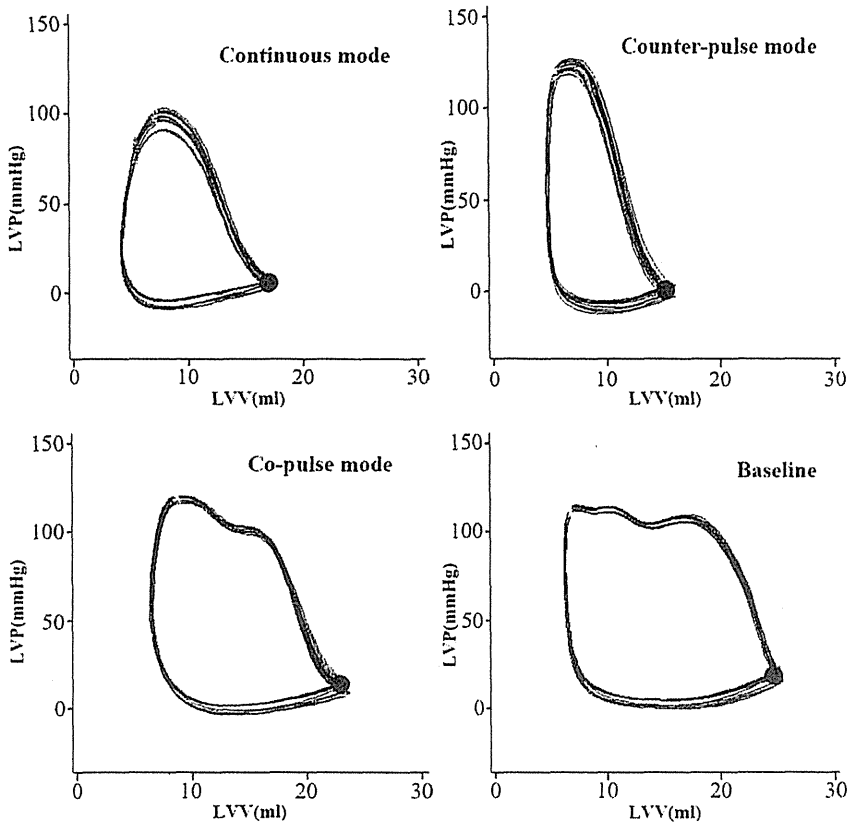

FIGURE 2. Pressure–volume loops at full bypass at baseline and for each mode. The end-diastolic point is shown by the *black dot*. In the co-pulse mode, the end-diastolic points had shifted rightward compared with those in the continuous mode and had a value that was similar to baseline. In the counterpulse mode, the end-diastolic points had shifted leftward and decreased compared with those in the continuous mode. Furthermore, the pressure–volume loop area was increased in the co-pulse mode and decreased in the counterpulse mode compared with that in the continuous mode. *LVV*, Left ventricular volume; *LVP*, left ventricular pressure.

in the conscious state than in the anesthetized state. Second, we simply compared the effects of the different NHLCS modes in the present study, because we were not able to clamp the LVAD circuit to hold the PF constant. Third, we have demonstrated the effects of NHLCS in a chronic heart failure model.

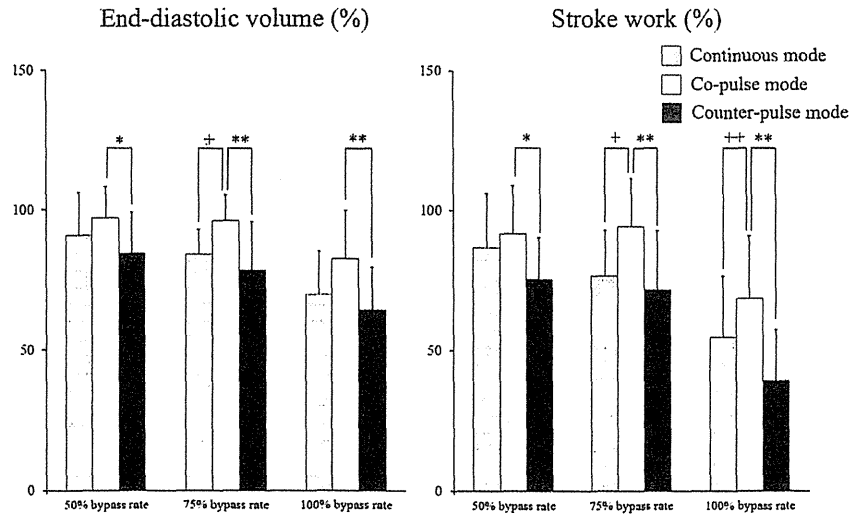

FIGURE 3. The left ventricular end-diastolic volume (LVEDV) and stroke work (SW) are shown relative to the baseline, which was obtained under 0% bypass (100%). A trend was seen for the percentage of LVEDV in the co-pulse mode to increase at each bypass rate and for the LVEDV in the counterpulse mode to decrease compared with that in the continuous mode. In addition, a similar trend was seen for the percentage of SW in the co-pulse mode to increase at each bypass rate and for the SW in the counterpulse mode to decrease compared with that in the continuous mode. *,+$P < .05$; ++,**$P < .01$.

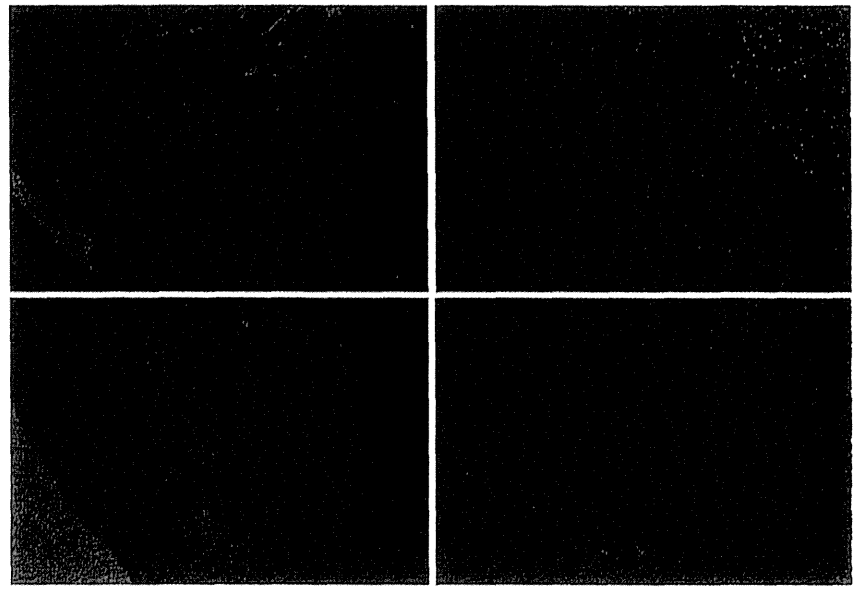

FIGURE 4. Myocardial hematoxylin and eosin stain, (A and B) before, and (C and D) after left ventricular assist device implantation. *Scale bars* represent (A and C) 500 μm and (B and D) 50 μm.

Recently, it has become clear that electrocardiogram-synchronized RS control systems have beneficial effects on cardiac load and hemodynamics. Significant controversy has resulted regarding the differences between pulsatile and nonpulsatile hemodynamics.[19-23] Our system can generate artificial pulsatility, in addition to the beneficial effects on the cardiac workload.[8] In addition, Kishimoto and colleagues[24] reported that speed modulation can open the aortic valve and might prevent aortic insufficiency. Furthermore, Ando and colleagues[25,26] reported that to prevent backward flow, it is possible to increase the RS in the diastolic phase and thus create a circuit clamp condition resembling the "off-test mode." We believe that the NHLCS has the potential to improve the success rate of cardiac recovery and allow more options in the treatment of patients with an implanted rotary blood pump.

Our study had several limitations. We used an animal model of LV dysfunction that showed decreased contractility. However, the EF did not actually decrease to a level that would warrant LVAD implantation in a clinical setting. To compare the effect of different NHLCS operating modes, it would be better to use an impaired cardiac function model.[10] In addition, we did not show actual myocardial recovery, because we tested the NHLCS for 12 hours, which was not long enough to evaluate recovery. However, we have developed a program for the NHLCS that will make it suitable for long-term use. We are currently investigating the actual long-term effects of this system on cardiac recovery and adverse events in a chronic heart failure model.

CONCLUSIONS

We have shown that the NHLCS can actively control the LV load in a chronic heart failure model. The NHLCS can provide a favorable LV load in each phase of cardiac recovery, contributing to an increase in the success rate of BTR therapy.

The authors are grateful to Dr Daisuke Ogawa in the Sun Medical Technology Research Corporation for creating the programs.

References

1. Slaughter MS, Rogers JG, Milano CA, Russell SD, Conte JV, Feldman D, et al. Advanced heart failure treated with continuous-flow left ventricular assist device. *N Engl J Med*. 2009;361:2241-51.
2. Starling RC, Naka Y, Boyle AJ, Gonzalez-Stawinski G, John R, Jorde U, et al. Results of the post-US Food and Drug Administration-approval study with a continuous flow left ventricular assist device as a bridge to heart transplantation: a prospective study using the INTERMACS (Interagency Registry for Mechanically Assisted Circulatory Support). *J Am Coll Cardiol*. 2011;57:1890-8.
3. Kitamura S. Heart transplantation in Japan: a critical appraisal for the results and future prospects. *Gen Thorac Cardiovasc Surg*. 2012;60:639-44.
4. Frazier OH, Benedict CR, Radovancevic B, Bick RJ, Capek P, Springer WE, et al. Improved left ventricular function after chronic left ventricular unloading. *Ann Thorac Surg*. 1996;62:675-81.
5. Maybaum S, Mancini D, Xydas S, Starling RC, Aaronson K, Pagani FD, et al. Cardiac improvement during mechanical circulatory support: a prospective multicenter study of the LVAD working group. *Circulation*. 2007;115:2497-505.
6. Kinoshita M, Takano H, Taenaka Y, Mori H, Takaichi S, Noda H, et al. Cardiac disuse atrophy during LVAD pumping. *ASAIO Trans*. 1988;34:208-12.
7. Yamazaki K, Kihara S, Akimoto T, Tagusari O, Kawai A, Umezu M, et al. EVAHEART: an implantable centrifugal blood pump for long-term circulatory support. *Jpn J Thorac Cardiovasc Surg*. 2002;50:461-5.
8. Ando M, Nishimura T, Takewa Y, Yamazaki K, Kyo S, Ono M, et al. Electrocardiogram-synchronized rotational speed change mode in rotary pumps could improve pulsatility. *Artif Organs*. 2011;35:941-7.
9. Ando M, Nishimura T, Takewa Y, Ogawa D, Yamazaki K, Kashiwa K, et al. A novel counterpulse drive mode of continuous-flow left ventricular assist devices

can minimize intracircuit backward flow during pump weaning. *J Artif Organs.* 2011;14:74-9.
10. Umeki A, Nishimura T, Ando M, Takewa Y, Yamazaki K, Kyo S, et al. Alteration of LV end-diastolic volume by controlling the power of the continuous-flow LVAD, so it is synchronized with cardiac beat: development of a native heart load control system (NHLCS). *J Artif Organs.* 2012;15:128-33.
11. Dixon JA, Spinale FG. Large animal models of heart failure: a critical link in the translation of basic science to clinical practice. *Circ Heart Fail.* 2009;2: 262-71.
12. Umeki A, Nishimura T, Takewa Y, Ando M, Arakawa M, Kishimoto Y, et al. Change in myocardial oxygen consumption employing continuous-flow LVAD with cardiac beat synchronizing system, in acute ischemic heart failure models. *J Artif Organs.* 2013;16:119-28.
13. Kono S, Nishimura K, Yamada T, Oonishi T, Tsukiya T, Akamatsu T, et al. In vivo and in vitro evaluation of the pulsatile mode of a magnetically suspended centrifugal pump. *ASAIO J.* 1997;43:M580-4.
14. Ando M, Takewa Y, Nishimura T, Yamazaki K, Kyo S, Ono M, et al. A novel counterpulsation mode of rotary left ventricular assist devices can enhance myocardial perfusion. *J Artif Organs.* 2011;14:185-91.
15. Pirbodaghi T, Axiak S, Weber A, Gempp T, Vandenberghe S. Pulsatile control of rotary blood pumps: does the modulation waveform matter? *J Thorac Cardiovasc Surg.* 2012;144:970-7.
16. Pirbodaghi T, Weber A, Axiak S, Carrel T, Vandenberghe S. Asymmetric speed modulation of a rotary blood pump affects ventricular unloading. *Eur J Cardiothorac Surg.* 2013;43:383-8.
17. Hon JK, Yacoub MH. Bridge to recovery with the use of left ventricular assist device and clenbuterol. *Ann Thorac Surg.* 2003;75:S36-41.
18. Soppa GK, Lee J, Stagg MA, Felkin LE, Barton PJ, Siedlecka U, et al. Role and possible mechanisms of clenbuterol in enhancing reverse remodelling during mechanical unloading in murine heart failure. *Cardiovasc Res.* 2008;77: 695-6.
19. Nishimura T, Takewa Y, Huang Y, Shirota K, Ramanathan I, Hunyor S. Influence of varying conduit resistance on native heart function with nonpulsatile left heart bypass. *J Artif Organs.* 2001;4:126-30.
20. Nishimura T, Tatsumi E, Nishinaka T, Taenaka Y, Masuzawa T, Nakata M, et al. Diminished vasoconstrictive function caused by long-term nonpulsatile left heart bypass. *Artif Organs.* 1999;23:722-6.
21. Nishimura T, Tatsumi E, Nishinaka T, Taenaka Y, Nakata M, Takano H. Prolonged nonpulsatile left heart bypass diminishes vascular contractility. *Int J Artif Organs.* 1999;22:492-8.
22. Nishimura T, Tatsumi E, Taenaka Y, Nishinaka T, Nakatani T, Masuzawa T, et al. Effects of long-term nonpulsatile left heart bypass on the mechanical properties of the aortic wall. *ASAIO J.* 1999;45:455-9.
23. Nishinaka T, Tatsumi E, Nishimura T, Shioya K, Ohnishi H, Taenaka Y, et al. Change in vasoconstrictive function during prolonged nonpulsatile left heart bypass. *Artif Organs.* 2001;25:371-5.
24. Kishimoto Y, Takewa Y, Arakawa M, Umeki A, Ando M, Nishimura T, et al. Development of a novel drive mode to prevent aortic insufficiency during continuous-flow LVAD support by synchronizing rotational speed with heartbeat. *J Artif Organs* 2013;129-37.
25. Ando M, Nishimura T, Takewa Y, Ogawa D, Yamazaki K, Kashiwa K, et al. What is the ideal off-test trial for continuous-flow ventricular-assist-device explantation? Intracircuit back-flow analysis in a mock circulation model. *J Artif Organs.* 2011;14:70-3.
26. Ando M, Nishimura T, Takewa Y, Kyo S, Ono M, Taenaka Y, et al. Creating an ideal "off-test mode" for rotary left ventricular assist devices: establishing a safe and appropriate weaning protocol after myocardial recovery. *J Thorac Cardiovasc Surg.* 2012;143:1176-82.

International Journal of Fluid Machinery and Systems
Vol. 7, No. 4, October-December 2014

DOI: http://dx.doi.org/10.5293/IJFMS.2014.7.4.142
ISSN (Online): 1882-9554

Original Paper

Study on the Development of Two-Stage Centrifugal Blood Pump for Cardiopulmonary Support System

Hironori Horiguchi[1], Tomonori Tsukiya[2], Takeshi Nomoto[1], Toratarou Takemika[1], and Yoshinobu Tsujimoto[1]

[1]Graduate School of Engineering Science, Osaka University
1-3 Machikaneyama, Toyonaka, Osaka, 560-8531, Japan
[2]Department of Artificial Organs, National Cerebral and Cardiovascular Center
5-7-1 Fujishirodai, Suita, 565-8565

Abstract

In the cardiopulmonary support system with an ECMO (extracorporeal membrane oxygenation), a higher pump head is demanded for a blood pump. In order to realize a blood pump with higher pump head, higher anti-hemolysis and thrombosis performances, a study on the development of unprecedented multistage blood pump was conducted. In consideration of the application of the blood pump for pediatric patients, a miniature two-stage centrifugal blood pump with the impeller's diameter of 40mm was designed and the performance was examined in experiments and computations. Some useful knowledge for a design of the blood pump with higher anti-hemolysis and thrombosis performances was obtained.

Keywords: Centrifugal Pump, Artificial Heart, Blood, Hemolysis, Thrombosis

1. Introduction

Blood pumps for the cardiopulmonary support system with an ECMO (extracorporeal membrane oxygenation) need a higher pump head of approximately 200-500mmHg due to high pressure losses in the membrane oxygenator and the cannula tubing. Existing single stage centrifugal pumps can generate the higher pump head with higher rotational speed of the impeller. However, the large shear stress due to the higher rotational speed can occur and lead to a mechanical hemolysis (destruction of red blood cells). In severe conditions of the higher pump head of 500 mmHg, the hemolysis could occur even in the Jostra RotaFlow centrifugal pump, which is considered to have high anti-hemolysis performance [1]. The cases where the hemolysis becomes a problem have been reported for pediatric patients using the ECMO [2].

In order to realize a blood pump with higher pump head, higher anti-hemolysis and thrombosis performances, a basic study on the development of unprecedented multistage blood pump was conducted. In consideration of the application of the blood pump for pediatric patients, a miniature two-stage centrifugal blood pump with the impeller's diameter of 40mm was designed and the performance test was conducted. The simulation of the internal flow was also made and the problem to solve was extracted. Some useful knowledge for a design of the blood pump with higher anti-hemolysis and thrombosis performances was obtained and reported in the present paper.

2. Design of Pump

In the design of blood pumps, we need to consider the suppression of hemolysis and thrombosis. The type number of blood pumps is low in general and the design method of blood pumps has not been established yet. In the present study, based on the design method of general industrial centrifugal pumps, a novel two-stage centrifugal blood pump has been designed, using the knowledge of the suppression of hemolysis and thrombosis for single-stage blood pumps. The flow rate, the pump head, and the rotational speed at the design point are 3 L/min, 500 mmHg, and 4200 rpm, respectively.

The meridian cross-section of the designed blood pump are shown in Fig.1. The cross-sections from A to F in Fig.1 are shown in Fig.2. The working fluid flows into the suction volute shown in Fig.2(a), and flows through the first-stage impeller (Fig.2(c)), the return channel (Fig.2(d)), the second-stage impeller (Fig.2(f)), and the double volute (Fig.2(f)) and flows out from the pump. The suction volute (Fig.2(a)) generates a pre-swirl flow at the inlet of the impeller in the opposite direction of the rotation of the impeller for higher pump head. The double volute casing (Fig.2(f)) was adopted to decrease the radial fluid force acting on the impeller, considering the change of the present pump into a magnetically-levitated pump in the future. The casing is made of a transparent

Received May 2 2014; accepted for publication June 2 2014: Review conducted by Prof. Xuelin Tang. (Paper number O14010C)
Corresponding author: Hironori Horiguchi, Associate Professor, horiguti@me.es.osaka-u.ac.jp

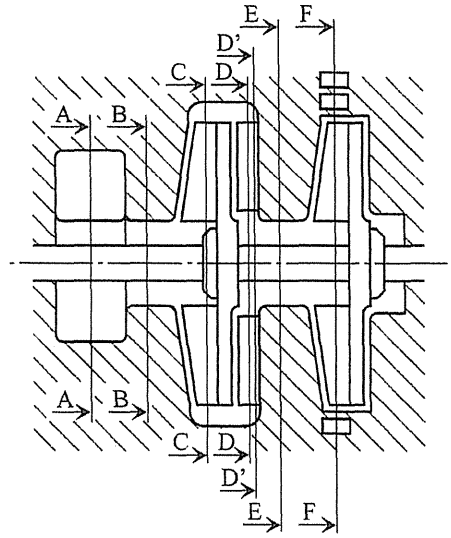

Fig. 1 Meridian cross-section of the blood pump

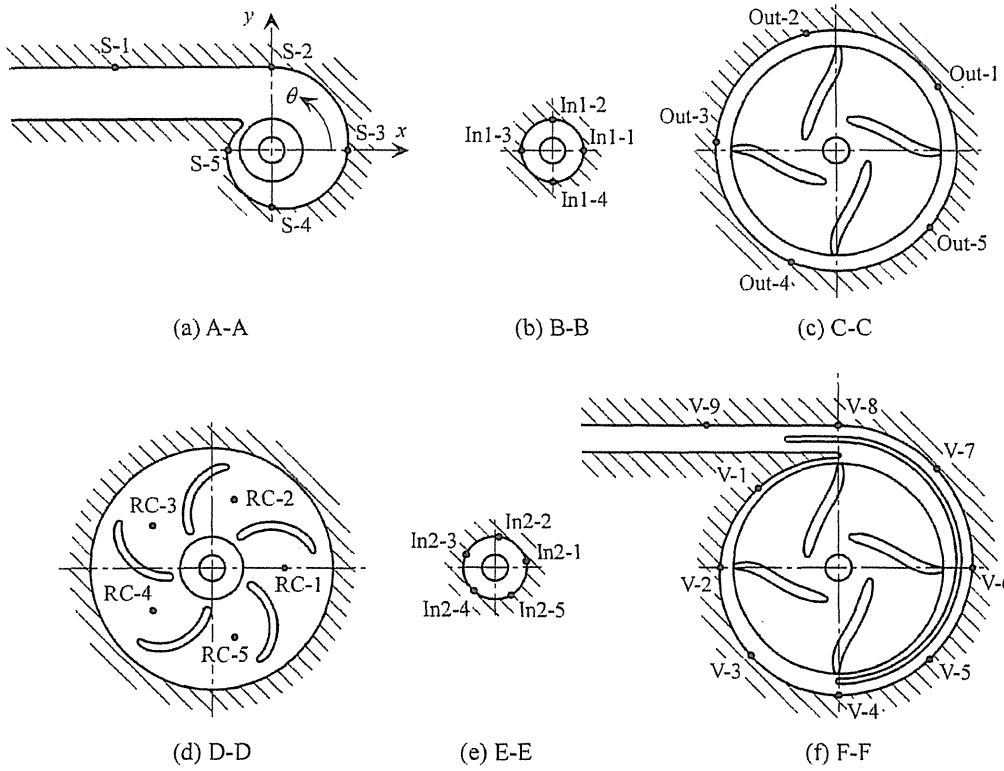

(a) A-A (b) B-B (c) C-C

(d) D-D (e) E-E (f) F-F

Fig. 2 Cross-section of the pump and the position of holes for the measurement of pressure distribution

acrylic resin for a visual observation. The black dots in Fig.2 show the measuring points of pressure and their names are shown on the side of them.

The specification of the pump is shown in Table 1. To suppress the stagnation near the tip of blades, a semi-open type impeller was adopted. The diameter D_t of the impeller is 40 mm and the pump has a small priming volume of 42 ml. The shapes of the blades of the 1st and 2nd stage impellers are the same and two-dimensional. The inlet and outlet blade angles, β_1 and β_2, are 4.7 deg and 80 deg, respectively. The inlet blade angle is small and 4 blades are given to the impeller so that the blades do not choke the flow passage at the inlet. The geometry of the blade was designed by a three-circular-arc method.

It is pointed out in some studies that there is an optimum tip clearance to prevent the hemolysis. In the study of Schima et al. [4], the tip clearance of 1.5mm leads to the minimum amount of hemolysis in a single stage centrifugal pump with an impeller similar to the present pump impeller, although a shear velocity in the tip clearance around the periphery of the impeller in the reference [4] is low and about 27% (2300 s^{-1}) of the shear velocity of 8400 s^{-1} in the present pump. In the studies of Miyazoe et al. [5] and

Table 1 Specification of the pump

Type of impeller	Semi-open
Number of blade	4
Diameter of impeller, D_t [mm]	40
Inlet blade angle, β_1 [deg]	4.7
Outlet blade angle, β_2 [deg]	80.0
Blade height at the inlet, h_1[mm]	5.0
Blade height at the outlet, h_2[mm]	3.0
Tip clearance, C [mm]	1.0
Design flow rate, Q_d [L/min]	3.0
Design pump head [mmHg]	500

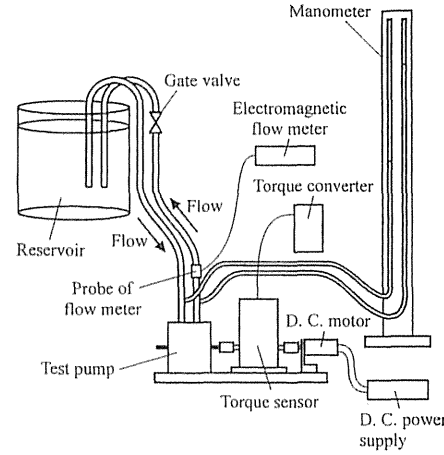

Fig. 3 Experimental setup for the measurement of pump performance and pressure distribution

Masuzawa et al. [6], the effect of the tip clearance was examined and it was found that the shear stress in the fluid and the amount of hemolysis significantly decrease by changing the tip clearance from 0.5 mm to 1 mm. In the cases with the tip clearances of 1mm and 1.5 mm, there was no difference of the shear stress and the amount of hemolysis. Therefore, the tip clearance C of 1 mm was adopted in the present study.

Assuming that each stage of the pump generates a half of total pump head, the pump in each stage has a low type number of 0.13 (specific speed is 92 (rpm, m^3/min, m)). Based on the design method for general industrial pumps, the blade heights at the inlet and the outlet, h_1 and h_2, are 3 mm and 1 mm, respectively. In comparison with the tip clearance of 1 mm, the blade heights are quite small and it was expected that the internal flow in the impeller was disturbed by the leakage flow though the tip clearance. Therefore, the blade heights, h_1 and h_2, were increased to 5 mm and 3 mm, respectively, and the effect of the leakage flow to the internal flow was relatively decreased. In the return channel shown in Fig.2(d), five guide vanes with the inlet blade angle of 2 deg and the outlet blade angle of 90 deg are given.

3. Experiment

Schematic of the experimental apparatus for the measurement of pump performance and pressure distributions inside the pump are shown in Fig.3. The working fluid is a water at ordinary temperatures. The water flows from the reservoir, passes through the suction tube, the pump, the discharge tube, and returns to the reservoir. To measure the pressure in the suction and discharge tubes and the inside of the pump, a water column manometer was used. For the measurement of the flow rate, the magnetic flow meter (Nihon Kohden Corporation, MFV-3200) is set in the discharge tube. The flow rate was adjusted by clamping the discharge tube or the gate valve. The pump was driven by the DC motor (Maxon motor, RE30). For the measurement of the torque, the torque meter (Ono Sokki Co., Ltd., MD-503C) was used. The rotational speed of the pump was measured by the optical detector (Ono Sokki Co., Ltd., LG-9200) and displayed by the digital tachometer (Ono Sokki Co., Ltd., TM-2110). The rotational speed of the pump was set to be 1200 rpm or 1150 rpm so that the Reynolds number Re ($\equiv U_t D_t / \nu$) in the experiment using the water at ordinary temperatures was equal to be about 1.1×10^6 in the operation at the rotational speed of 4200rpm or 4000rpm with the blood assuming the density ρ of 1050 kg/m^3, the viscosity μ of 3.25 m·Pa·s (kinetic viscosity ν of 3.1×10^{-6} m^2/s).

4. Computation

For the simulation of the flow, a commercial software, ANSYS CFX-11.0 was used. The governing equations are the continuity equation and the Reynolds averaged Navier-Stokes equation. The k-ω turbulence model was used.

The computational domain consists of a rotational domain of the impeller and stationary domains of the casing, the suction and discharge tubes. The computational grid on the surface of the computational domain is shown in Fig.4. The shape of computational cell is tetrahedral in almost all of the computational domains and triangular prism near the wall. The maximum values of y^+ were about 14. Therefore, ω for the viscous sublayer or the blending expression of ω for the region between the viscous sublayer and the logarithmic layer was automatically selected in the computation [7, 8]. The number of cells are about 240,000, 460,000, 30,000, 30,000 for the domains of the impeller, the casing, the suction tube, and the discharge tube, respectively, and totally about 760,000. The static pressure at the inlet, the mass flow rate at the outlet, the non-slip condition on the wall were given as boundary conditions. The unsteady flow simulation was conducted with the time step of one hundredth of the rotational period. The working fluid is a water at ordinary temperatures and the rotational speed is 1200 rpm or 1150 rpm, as in the experiment.

For a pump similar to the present pump, the simulations with the computational cells of about 1.2 million or 3 million were conducted. The wall shear stress was a little larger in the case with larger number of cells. However, the distributions of the wall shear stress had no large difference qualitatively. Thus, in the view of the computational cost, the computational grid with the smaller number of cells was adopted.

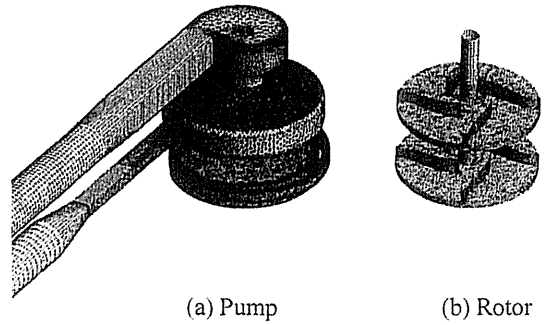

(a) Pump (b) Rotor

Fig. 4 Computational grid on the pump and the rotor

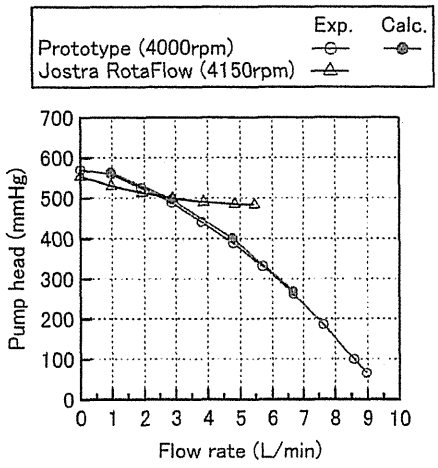

Fig. 5 Pump performance

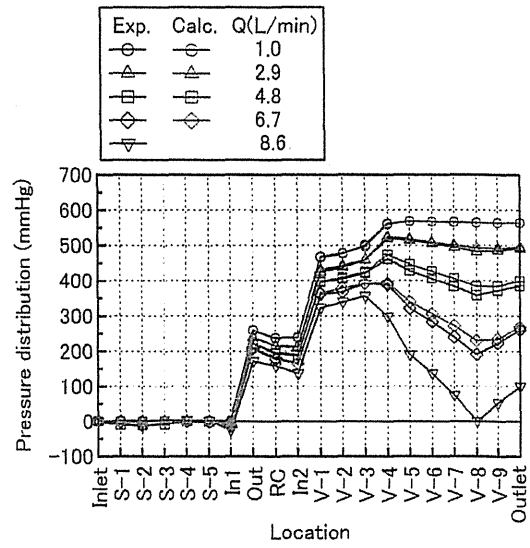

Fig. 6 Pressure distribution in the pump

5. Results and Discussions

5.1 Performance Curve

Figure 5 shows a performance curve of the prototype. The horizontal and vertical axes mean the flow rate and the pump head, respectively. The experiment was conducted with the rotational speed of 1200 rpm using the water and the results were converted into the values in the operation with the blood at 4000 rpm, considering an easy understanding in clinical practice. The demanded pump performance of 500 mmHg at 3 L/min was obtained at 4000 rpm in the experiment with the blood, although the design rotational speed was 4200 rpm. Therefore, the results were converted into the values at 4000 rpm, using the relation of $\Delta p_{blood} = \Delta p_{water} \cdot \rho_{blood} \cdot U_{t,blood}^2 / (\rho_{water} \cdot U_{t,water}^2)$ derived from the condition that the values of the pressure coefficients in the operations with the water and the blood are the same because the Reynolds numbers are equal and the flow fields are hydrodynamically similar in both cases.

As a reference pump, the Jostra RotaFlow centrifugal pump (Maquet Cardiopulmonary AG) was used, which is of practical use and is considered to have high anti-hemolysis performance. The pump performance of the Jostra RotaFlow centrifugal pump is also shown in Fig.5. The results was obtained through translating the results of 1200 rpm with the water into the results of 4150 rpm with the blood. The slope of the performance curve of the prototype is steeper than that of the Jostra RotaFlow centrifugal pump in usable ranges of 1 - 5 L/min. This means that the prototype has useful characteristics that the flow rate is insensitive to the flow resistance. The results of the CFD for the prototype is also shown in Fig.5 and agree with experimental results well.

The efficiency of the prototype was also measured. As the torque generated by the friction between the shaft and the seal was different case by case in the operation using the air as a working fluid, there was variation in the efficiency obtained by substituting the torque with the air from that with the water. In the operation using the water, the torque generated by the friction between the shaft and the seal was stable. The efficiency including the friction between the shaft and the seal was 5 - 8 % at $Q=Q_d$ (3 L/min) and the maximum efficiency was 6 - 10 % at 5 L/min.

5.2 Pressure Distribution

The pressure distribution in the pump was measured at 0.29, 0.86, 1.43, 2.00, 2.57 L/min at 1200 rpm and shown in Fig.6. These

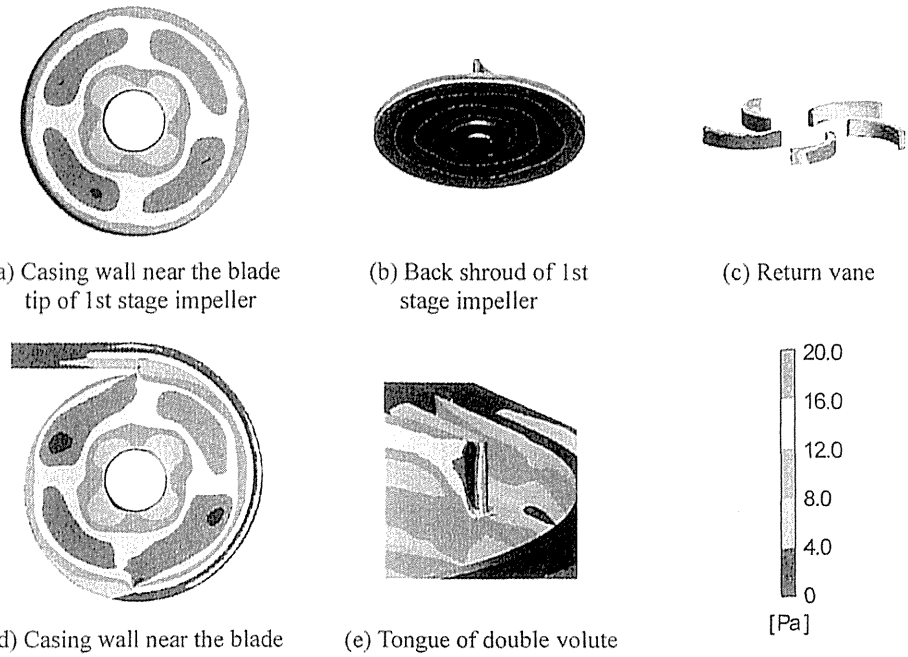

(a) Casing wall near the blade tip of 1st stage impeller

(b) Back shroud of 1st stage impeller

(c) Return vane

(d) Casing wall near the blade tip of 2nd stage impeller

(e) Tongue of double volute

Fig. 7 Wall shear stress distribution in the pump at $Q=Q_d$. N=1150 rpm

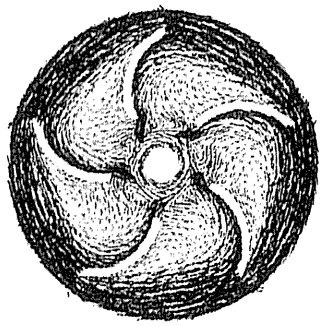

Fig. 8 Velocity vector on the cross-section (D'-D' in Fig.1) of the return channel at $Q=Q_d$. N=1150 rpm. The distance of the cross-section D'-D' from the casing wall is 0.5 mm.

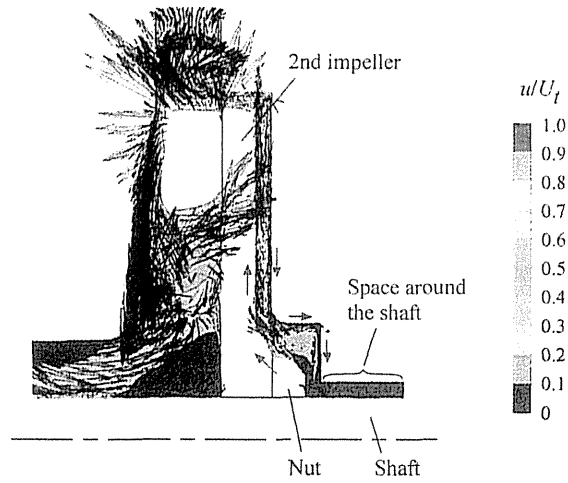

Fig. 9 Flow field on the meridian plane around the rear space of the back shroud of the 2nd stage impeller at $Q=Q_d$. N=1150 rpm.

flow rates corresponds to 1.0, 2.9, 4.8, 6.7, 8.6 L/min at the operation of 4000 rpm using the blood as a working fluid. The horizontal axis means positions shown in Fig.2. The values of In 1, Out, RC, In 2 are the averaged values of circumferential pressure distribution. The computational results are in good agreement with the experimental results except for the positions from V-5 to V-9 at higher flow rates (4.8 L/min and 6.7 L/min).

The pump head generated by the 1st and 2nd stage impellers are nearly same due the pre-swirl flow in the suction volute and the incomplete turning in the return guide vane. The pressure recovers smoothly in the double volute (V-1 to V-4) except for the case with the higher flow rate of 8.6 L/min.

5.3 Anti-Hemolysis Performance

Kameneva et al. [9] examined the blood flow in a narrow tube with the inner diameter of 1 mm and showed that the amount of the hemolysis drastically increased when the shear stress on the blood was larger than 200 Pa. Therefore, the shear stress of 200 Pa

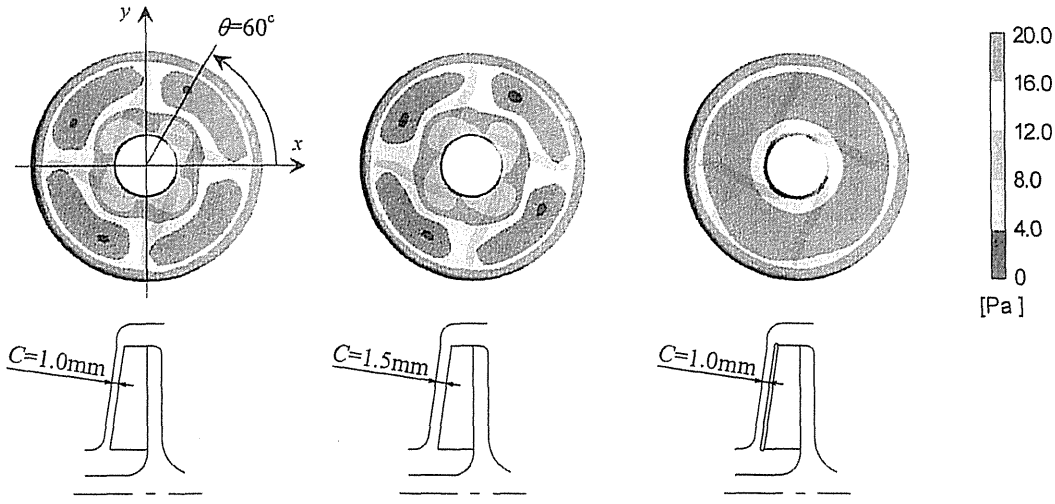

(a) C=1 mm (b) C=1.5 mm (c) C=1 mm with front shroud

Fig. 10 The effects of tip clearance and front shroud for wall shear stress on the casing wall near the 1st stage impeller. N=1150 rpm

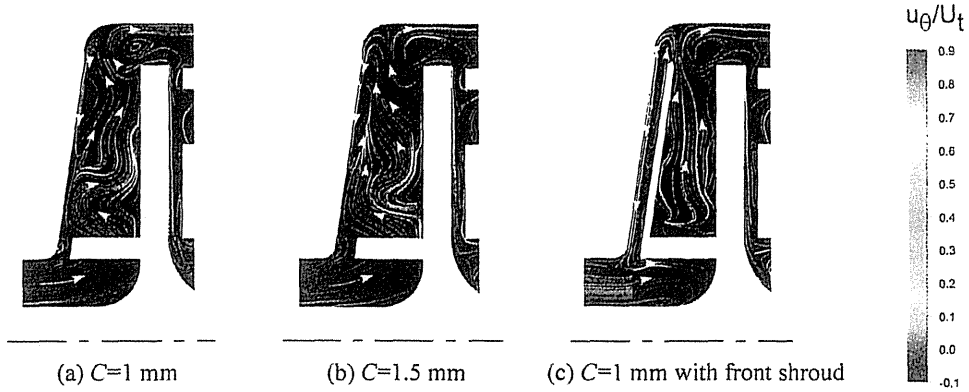

(a) C=1 mm (b) C=1.5 mm (c) C=1 mm with front shroud

Fig. 11 Streamline on meridian plane around the 1st stage impeller at θ=60 deg, defined in Fig.10(a)

was used as a threshold of hemolysis in the present study. The wall shear stress in the pump is shown in Fig.7. In the operation of 1150 rpm with the water, the threshold of the shear stress for the hemolysis is about 16 Pa, based on the similarity law of $\tau_{water} = \tau_{blood} \cdot \rho_{water} \cdot U_{t,water}^2 / (\rho_{blood} \cdot U_{t,blood}^2)$. The shear stress larger than 16 Pa is observed on the casing wall near the tip of the 1st and 2nd impellers (Fig.7(a) and (d)), the periphery of the backshroud of the 1st impeller (Fig.7(b)), and the tongue of the double volute casing (Fig.7(e)). The reduction of these high shear stress is necessary to suppress the hemolysis.

5.4 Anti-Thrombosis Performance

Figure 8 shows the velocity vector on the cross-section D'-D' in Fig.1, which is in the return channel and near the casing wall (0.5 mm from the wall). As shown in Fig.8, the flow separates from the blade and the stagnation occurs in the center of the vortex, which can cause the thrombosis.

Figure 9 shows the flow field in the meridian cross-section around the clearance between the backshroud of the 2nd impeller and the casing. The fluid in the boundary layer of the backshroud flows outward, driven by the centrifugal force due to the rotation of the impeller. The outward flow generates the inward flow near the casing, the recirculating flow occurs in the clearance. However, as the velocity is small near the shaft, it was suggested that the 2nd impeller should have a washout hole to suppress the thrombosis. The velocity in the space around the shaft is also small and should be removed for the suppression of the thrombosis. The spaces with the possibility of the thrombosis will be removed in next prototype.

5.5 Reduction of the High Wall Shear Stress on the Casing Wall near the Blade Tip of the Impeller

It is considered that an optimal tip clearance exists for the suppression of the hemolysis. In the study of Schima et al. [4], the amount of the hemolysis became smallest in the case with the tip clearance of 1.5 mm in a single stage centrifugal pump. Therefore, we conducted the computation for the pump with the tip clearance of 1.5 mm. Figure 10 shows the wall shear stress on the casing

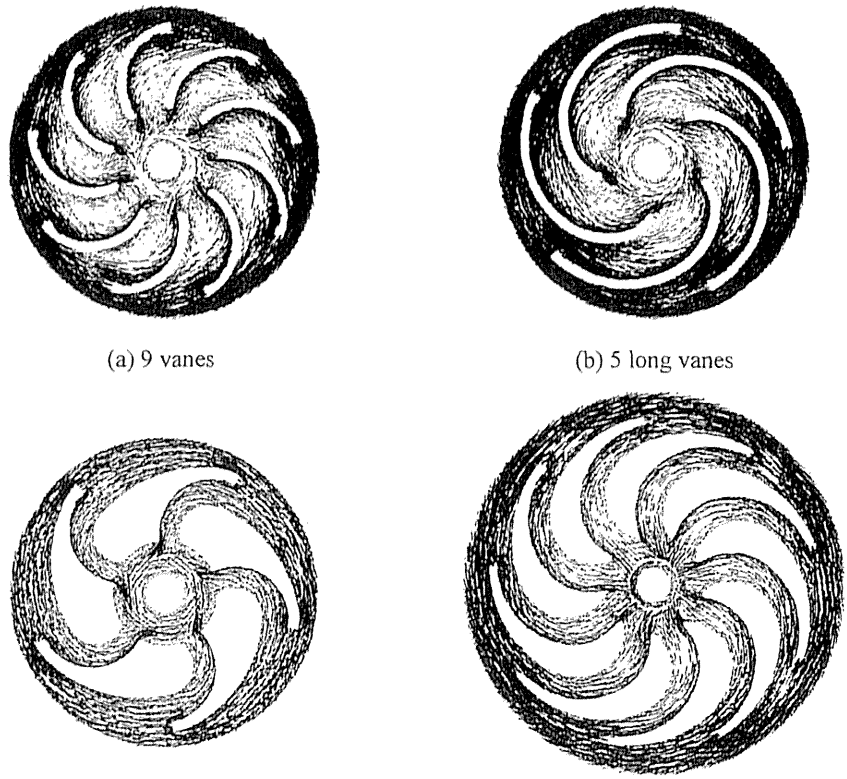

(a) 9 vanes (b) 5 long vanes

(c) 5 thicker vanes (d) 9 thicker vanes

Fig. 12 Velocity vector near the casing in various types of return guide vane (return channel)

near the blade tip of the 1st impeller. Figures 10 (a) and (b) show the results for C=1 mm and 1.5 mm, respectively. The results shown in Figs.7(a) and 10(a) are a little different due to the difference of the return channel. It could be confirmed that the region with the shear stress higher than 16 Pa decreases due to the increase of the tip clearance, but the amount of the reduction of high shear stress region was small. Figure 10(c) shows the results in the case of the impeller with a front shroud and the clearance of C = 1 mm. The front shroud was quite effective for reducing the high shear stress region.

Figure 11 shows streamlines around the 1st impeller on the meridian cross-section at θ=60 deg shown in Fig.10(a). The color of the streamlines means the ratio of the circumferential velocity u_θ to the tip speed U_t. Figures 11(a), (b), (c) show the results of C = 1 mm, 1.5 mm, and 1 mm with the front shroud, respectively. As shown in Figs.11(a) and (b), a larger circumferential velocity occurred near the casing wall around the tip of the impeller. This is the cause of the higher wall shear stress on the casing near the tip of the impeller. In the case with the front shroud, the occurrence of the higher velocity near the casing is suppressed as shown in Fig.11(c) and this leads to the suppression of the higher shear stress.

The pump head in the cases with C=1 mm, 1.5 mm, and 1 mm with the front shroud are 485 mmHg, 463 mmHg, and 538 mmHg, respectively, and the pump head increased by about 11% using the front shroud. Kurokawa et al. [10] reported that the head of the pump with a low specific speed increases using the front shroud. As the increase of the pump head results in a low rotational speed of the impeller, the front shroud has an advantage for the anti-hemolysis performance.

5.6 Modification of the Return Guide Vane

As shown in Fig.8, in the return channel, the stagnation which could be the cause of the thrombosis occurred at the center of the steady vortex due to the flow separation. Therefore, the geometry of the return guide vane (return channel) was considered to suppress the stagnation. The geometries of various types of the return guide vane (return channel) we considered and the velocity field were shown in Fig.12. The vane angles of pressure surface at the inlet and the outlet are 2 deg and 90 deg, respectively. To increase the effect of the return guide vane, the number of the vanes was increased from 5 to 9 and the flow field in the case with 9 guide vanes was shown in Fig.12(a). Although the size of the vortex diminished in comparison with Fig.8, the stagnation at the center of vortex due to the flow separation occurred.

The height of the return guide vane in the present study was larger so as to be equal to the larger blade height of the impeller. For this reason, the circumferential velocity is quite larger than the radial velocity in the return channel. Therefore, longer guide vane was tried to be adopted to turn the flow gradually from the circumferential direction to the radial direction. The flow field for the longer guide vane is shown in Fig.12(b). Larger flow separation was suppressed by the longer guide vane, but the flow was not along the guide vane near the outlet of the return channel and the circumferential velocity could not be decreased well. In the above modifications, the vane with a constant thickness was adopted for easy designing of the vane but was difficult to suppress the flow separation. Then, we gave the thickness to the guide vane such that the vane covers the region of the flow separation shown in Fig.8.